Anomalous violation of the local constant field approximation in colliding laser beams

Q. Z. Lv,* E. Raicher,† C. H. Keitel, and K. Z. Hatsagortsyan
Max-Planck-Institut für Kernphysik, Saupfercheckweg 1, 69117 Heidelberg, Germany

(Received 13 March 2020; revised 8 June 2020; accepted 9 February 2021; published 8 March 2021)

The local constant field approximation (LCFA) is widely used in the study of QED effects in laser-matter interactions, with the justification that the classical strong-field parameter of the impinging laser beam is large. Here, the failure of this conjecture is demonstrated for an electron interacting with strong counterpropagating laser waves due to the emergence of an additional small time scale in the electron dynamics. Moreover, we identify a class of anomalous LCFA violation in which electrons turn sharply and leave the radiation formation zone much earlier than in the LCFA estimation. In contrast to previous observations of LCFA violation in a single laser beam, resulting in new low-harmonic peaks in the spectrum, here deviations from LCFA results are seen across the whole spectrum. A similar phenomenon is also demonstrated for an electron colliding with an ultrashort laser pulse. These results indicate the necessity of amending laser-plasma kinetic simulations in multiple beam laser configurations.

DOI: 10.1103/PhysRevResearch.3.013214

I. INTRODUCTION

Exploration of novel regimes of laser-matter interaction, including nonlinear QED [1–10] and radiation reaction [11–13] effects, has been enabled due to the dramatic progress in high-power laser technology [14,15]. The peak power of contemporary lasers has currently attained the petawatt regime [16,17], and multipetawatt infrastructures are under construction worldwide [18,19].

Strong-field QED processes in laser fields can be treated fully quantum mechanically only for limited field configurations, where the single-particle wave function is available [20–23]. Therefore the standard Monte Carlo codes, which are employed for theoretical investigation of QED effects in laser-plasma interaction [24–27], treat photon emission and pair production within the local constant field approximation (LCFA).

The LCFA is commonly believed to be applicable in strong laser fields with $\xi \gg 1$, which follows from the more precise condition $(\xi/\chi^{1/3})[\omega/(\varepsilon-\omega)]^{1/3} \gg 1$ [28,29] using typical emission frequencies $\omega/\varepsilon \sim \chi/(\chi+1)$. Here, $\xi = |e|E_0/m\omega_0$ and $\chi = |e|\sqrt{-(F^{\mu\nu}P_\nu)^2}/m^3$ are the strong-field classical and quantum parameters [30], respectively. Starting from the foundations, the physical condition for the LCFA applicability is $t_f \ll t_c$, with the radiation formation time t_f and the characteristic time of the electron trajectory t_c [31,32]. As an ultrarelativistic electron emits forward within a $1/\gamma$ cone [33], the radiation can be superimposed and coherently formed during the formation time t_f spent by the electron in the $1/\gamma$ cone. While in a single laser field, $t_f/t_c \sim 1/\xi$ [34], in multibeam laser configurations several characteristic time scales can appear in the trajectory. As a result, the condition $t_f \ll t_c$ will not be equivalent to $\xi \gg 1$, and therefore violation of LCFA may arise even for $\xi \gg 1$. In common practice, however, the LCFA is applied for simulations of radiative processes in laser-plasma interaction when a strong laser field with $\xi \gg 1$ impinges on plasma, overlooking that during the interaction other electromagnetic modes such as reflected (e.g., from the critical density [35]) and/or plasma waves may arise, which can disturb the LCFA applicability.

Multibeam configurations are attractive for achieving the highest possible local fields with a given energy in the original laser beam, such as the configuration of the dipole wave [36–39], and for inducing various nonlinear QED processes [40–45]. Several multipetawatt facilities under construction, such as the ELI Laser Facility [46,47] and the SHINE Facility in China [48], enable a multipulse colliding scenario. Therefore the question of LCFA applicability in such configurations is an important issue. The simplest multibeam laser configuration is a setup of counterpropagating laser waves (CPWs), which exhibits radiative trapping dynamics [49,50].

Here, we show that for CPWs of the same frequency, two additional small characteristic time scales t_2 and t_3 emerge in the trajectory along with the fundamental one, t_1, corresponding to a single laser wave (see Fig. 1). In the case where these are comparable to the corresponding formation time scales, $t_{fi} \gtrsim t_i$, $i = 1, 2, 3$, a deviation from LCFA arises. With $t_c = |\boldsymbol{F}|/|\dot{\boldsymbol{F}}|$, where $\boldsymbol{F}$ is the Lorentz force, the shortest time scale t_3 corresponds to the parts of the trajectory where the force is relatively small but changing rapidly. It is due to counteracting contributions of the laser beams into the electron nonlinear dynamics and determined by the quantum

*qingzheng.lyu@mpi-hd.mpg.de
†Present address: Soreq Nuclear Research Center, Yavne 80800, Israel; erez.raicher@mail.huji.ac.il

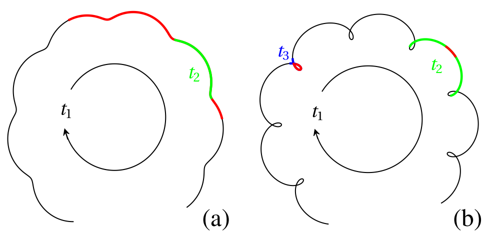

FIG. 1. Examples of electron trajectories in circularly polarized CPWs (projection on the plane transverse to the laser propagation): (a) $\xi_1 \gg 1$ and $\xi_2 < 1$ ($t_{f2} > t_2$); (b) $\xi_1 \gg \xi_2 \gg 1$ ($t_{f2} < t_2$, but $t_{f3} \approx t_3$). Red is the radiation formation length, and green and blue are the additional characteristic lengths of the electron trajectory [t_i and t_{fi} ($i = 1, 2, 3$) are the corresponding characteristic and formation times]. While in a single laser wave only t_1 is available, in CPWs additional small time scales arise. LCFA fails at $t_{fi} \gtrsim t_i$. In (a), $t_{f2} > t^L_{f2}$, while in (b), $t_{f3} < t^L_{f3}$, which represents a class of anomalous LCFA violation.

nonlinear parameters of the laser fields. In the regime of Fig. 1(a) the formation time is larger than that via LCFA (t^L_f), the electron oscillates fast within the radiation formation zone, the LCFA violation is similar to that in a plane laser wave at $\xi \lesssim 1$, and the spectrum is dominated by low harmonics of the Doppler-shifted oscillation frequency (the corrections to LCFA for this type of violation, with $t_f > t^L_f$, are considered in Refs. [51,52]). In contrast, in the regime of Fig. 1(b) the electron motion during t_3 is extremely abrupt, accompanied with a comparable formation time $t_f \sim t_3$, and leaving the formation zone (the $1/\gamma$ cone) much earlier than within the LCFA: $t_f < t^L_f$. In this case, the LCFA failure will be exhibited by the appearance of a large characteristic frequency in the spectrum due to a small t_f; that is, the spectrum will deviate from that via the LCFA in the high-energy region.

The deviations from LCFA results presented in Fig. 1(b) essentially differ from those in the infrared tail of the spectrum for a plane laser wave discussed in Refs. [28,53,54]. There, the condition $t^L_f \ll t_c$ is fulfilled, and the LCFA describes the main part of the spectrum very well. The deviation from LCFA calculations was observed only at low frequencies, where the coherence time is significantly longer, sampling the varying field beyond the formation time.

In this paper we explore the electron quantum radiation in CPWs in the realm of the Baier-Katkov (BK) semiclassical formalism [31,55,56]. We describe the concept and identify the regimes of LCFA violation beyond $\xi \gg 1$. The calculations via BK formalism employ the classical electron trajectory; however, they account for the quantum recoil due to a photon emission. We are interested in a situation when a small time scale t_c appears in the electron trajectory, which is the case when the force $\mathbf{F}$ and, consequently, the time-dependent quantum parameter $\chi(t)$ become small at certain points of the trajectory and further change rapidly. This can be achieved in two scenarios in the CPW configuration. In the first one, an electron moves relativistically along the propagating axis of the CPW, and the quantum parameters regarding each laser pulse χ_1 and χ_2 are of the same order of magnitude. This gives us the relationship between different parameters as $(1-\bar{\beta}_z)\xi_1 \approx (1+\bar{\beta}_z)\xi_2$, where $\bar{\beta}_z$ is the z component of the average velocity for the electron during the interaction. To fulfill the required condition $\chi_1 \sim \chi_2$, we consider $\xi_1 \gg \xi_2$ with an electron copropagating with the strong wave. For this case, an analytical model is developed and validated by a full numerical calculation. In the other one, an electron is trapped around the antinode of a standing wave formed by the CPW with $\xi_1 > \xi_2$. We avoid the case of $\xi_1 \approx \xi_2$ because $\chi(t)$ is almost constant at the antinode of a standing wave with equal field strength, where only a magnetic field exists, and also to refrain from the chaotic dynamics. We consider two qualitatively different regimes for an ultrarelativistic electron moving along the wave propagation direction: $\xi_1 \gg 1$ and $\xi_2 \lesssim 1$ [Fig. 1(a)] and $\xi_1 \gg \xi_2 \gg 1$ [Fig. 1(b)], with ξ_i ($i = 1, 2$) for the ith laser field. A significant deviation from the LCFA results is demonstrated in the high-energy domain of the radiation spectra for both regimes.

The case in Fig. 1(b) represents a typical example of the two-beam setup yielding the regime of a class of anomalous LCFA violation in which the particle leaves the $1/\gamma$ cone more rapidly than with the LCFA ($t_f < t^L_f$). Accordingly, the corresponding spectrum is broad and does not feature harmonics. Although in the case in Fig. 1(a) we have quite large modifications of the spectra with respect to LCFA, it represents the common regime of LCFA violation ($t_f \gtrsim t^L_f$), similar to the case of a relativistic electron counterpropagating a single laser beam with $\xi < 1$. The anomalous LCFA violation represented in Fig. 1(b) is also encountered in the electron interaction with an ultrashort pulse, where the new time scale is caused by the rapid changing of the pulse profile.

II. THEORETICAL DESCRIPTION

A. Electron dynamics in the CPW configuration

The classical equation of motion for the electron in the presence of electromagnetic (EM) fields reads

$$\frac{dP^\mu}{d\tau} = \frac{e}{m} F^{\mu\nu} P_\nu, \tag{1}$$

where τ is the proper time. The vector potential corresponding to the counterpropagating wave (CPW) configuration with circular polarization is $A^\mu = A^\mu_1 + A^\mu_2$, where

$$\begin{aligned} A^\mu_1 &\equiv a_1\left[\cos(\phi_1)e^\mu_x + \sin(\phi_1)e^\mu_y\right], \\ A^\mu_2 &\equiv a_2\left[\cos(\phi_2)e^\mu_x + \sin(\phi_2)e^\mu_y\right], \end{aligned} \tag{2}$$

with $e^\mu_x = (0, 1, 0, 0)$, $e^\mu_y = (0, 0, 1, 0)$ as the unit vectors. In the general case, Eq. (1) cannot be solved analytically because of its nonlinearity, which arises from the fact that $x_\mu(\tau)$ depends on the momentum via

$$x_\mu(\tau) = \int d\tau \frac{P_\mu(\tau)}{m}. \tag{3}$$

In the following, we seek an approximate solution to the equation of motion. The phases appearing in the EM field vector potential arguments can be written as

$$\begin{aligned} \phi_1(\tau) &\equiv k_1 \cdot x(\tau) = \frac{k_1 \cdot \bar{P}}{m}\tau + \delta\phi_1(\tau), \\ \phi_2(\tau) &\equiv k_2 \cdot x(\tau) = \frac{k_2 \cdot \bar{P}}{m}\tau + \delta\phi_2(\tau), \end{aligned} \tag{4}$$

with the four-wave-vectors of the beams as $k_1 = (\omega_0, 0, 0, \omega_0)$ and $k_2 = (\omega_0, 0, 0, -\omega_0)$. The bar symbol designates time-averaged quantities. The key assumption at the basis of our derivation is

$$\int \sin(\phi_i)d\tau \approx -\frac{m}{k_i \cdot \bar{P}}\cos(\phi_i),$$
$$\int \cos(\phi_i)d\tau \approx \frac{m}{k_i \cdot \bar{P}}\sin(\phi_i). \tag{5}$$

This means that the oscillating term $\delta\phi_1(\tau)$ and $\delta\phi_2(\tau)$ in the phase can be neglected during the integration. Applying this approximation, the momentum of the particle is

$$P_x(\tau) = m\xi_1\cos(\phi_1) + m\xi_2\cos(\phi_2),$$
$$P_y(\tau) = m\xi_1\sin(\phi_1) + m\xi_2\sin(\phi_2),$$
$$P_z(\tau) = \bar{P}_z + \frac{2m^2\xi_1\xi_2\omega_0}{(k_1-k_2)\cdot\bar{P}}\cos(\phi_1-\phi_2). \tag{6}$$

Here, $-ea_i = m\xi_i$ is considered, and a vanishing asymptotic transverse momentum $p_\perp = 0$ is chosen. The generalization to nonzero $p_\perp$ is straightforward. In order for Eq. (5) to be fulfilled, we need the oscillating term $\delta P_z = \frac{2m^2\xi_1\xi_2\omega_0}{(k_1-k_2)\cdot\bar{P}}\cos(\phi_1-\phi_2)$ to be much smaller compared with the average term,

$$\frac{\delta P_z}{\bar{P}_z} < \frac{\delta P_z}{\bar{\varepsilon}} = \frac{2m^2\xi_1\xi_2\omega_0}{(k_1-k_2)\cdot\bar{P}\bar{\varepsilon}} = \frac{m^2\xi_1\xi_2}{\bar{v}_z\bar{\varepsilon}^2} \ll 1. \tag{7}$$

Also, we assume $\xi_1 \gg \xi_2$ to avoid the chaos in the electron dynamics. With this, the energy of the particle looks like

$$\varepsilon = \left[m^2 + P_x^2 + P_y^2 + P_z^2\right]^{1/2}$$
$$= \left[m^2 + m^2\xi_1^2 + m^2\xi_2^2 + \bar{P}_z^2 + \delta P_z^2\right]^{1/2}. \tag{8}$$

Based on the condition in Eq. (7), the total energy is $\varepsilon = \sqrt{m_*^2 + \bar{P}_z^2} = \bar{\varepsilon}$ with the effective mass $m_* \equiv m\sqrt{1+\xi_1^2+\xi_2^2} \approx m\sqrt{1+\xi_1^2}$. The relation between the average energy and the asymptotic initial four-momentum p_0^μ seems therefore to be $\bar{\varepsilon} = \varepsilon_0 + m^2\xi_1^2/(\varepsilon_0 - p_{z0})$. Finally, the trajectory for an electron in the CPW configuration with circular polarization is

$$x(\tau) = \frac{m\xi_1}{k_1\cdot\bar{P}}\sin(\phi_1) + \frac{m\xi_2}{k_2\cdot\bar{P}}\sin(\phi_2),$$
$$y(\tau) = -\frac{m\xi_1}{k_1\cdot\bar{P}}\cos(\phi_1) - \frac{m\xi_2}{k_2\cdot\bar{P}}\cos(\phi_2),$$
$$z(\tau) = \frac{\bar{P}_z}{m}\tau + \frac{2m^2\xi_1\xi_2\omega_0}{[(k_1-k_2)\cdot\bar{P}]^2}\sin(\phi_1-\phi_2). \tag{9}$$

Since the velocity is $\boldsymbol{\beta}(\tau) = \boldsymbol{P}(\tau)/\varepsilon$, the acceleration can be written in terms of time t as

$$\dot{\beta}_x = -\frac{m\xi_1\omega_1}{\varepsilon}\sin\omega_1 t - \frac{m\xi_2\omega_2}{\varepsilon}\sin\omega_2 t,$$
$$\dot{\beta}_y = \frac{m\xi_1\omega_1}{\varepsilon}\cos\omega_1 t + \frac{m\xi_2\omega_2}{\varepsilon}\cos\omega_2 t,$$
$$\dot{\beta}_z = \frac{2\omega_0 m^2\xi_1\xi_2}{\varepsilon^2}\sin\Delta\omega t. \tag{10}$$

with $\omega_1 \equiv \omega_0(1-\bar{\beta}_z)$, $\omega_2 \equiv \omega_0(1+\bar{\beta}_z)$ and $\Delta\omega = \omega_1 - \omega_2$, where $\bar{\beta}_z = \bar{P}_z/\varepsilon$ is the average velocity along the z axis. Hence

$$\chi^2 = \frac{\gamma^4|\dot{\boldsymbol{\beta}}|^2}{m^2} = \chi_1^2 + \chi_2^2 - 2\chi_1\chi_2\cos\Delta\omega t$$
$$+ \frac{\xi_1^2\chi_2^2}{\gamma^2}\sin^2\Delta\omega t. \tag{11}$$

The last term is negligible, since $\xi_1 \ll \gamma$. Thus the expression appearing in Eq. (11) is obtained,

$$\chi \approx \sqrt{\chi_1^2 + \chi_2^2 - 2\chi_1\chi_2\cos\Delta\omega t}. \tag{12}$$

We further calculate the characteristic time of the electron trajectory $t_c = |\boldsymbol{F}|/|\dot{\boldsymbol{F}}|$, where $\boldsymbol{F}$ is the Lorentz force. Since the energy in Eq. (8) is constant, this quantity may be equivalently written as $t_c = |\dot{\boldsymbol{\beta}}|/|\ddot{\boldsymbol{\beta}}|$. The acceleration $\dot{\boldsymbol{\beta}}$ was already found, and the denominator $\ddot{\boldsymbol{\beta}}$ is straightforwardly obtained by taking a derivative of Eq. (10); hence the trajectory's characteristic time takes the form

$$t_c \approx \frac{\chi(t)}{\sqrt{\omega_1^2\chi_1^2 + \omega_2^2\chi_2^2 - 2\chi_1\chi_2\omega_1\omega_2\sin\Delta\omega t}}. \tag{13}$$

In the cases $\chi_1 \sim \chi_2$ and $\omega_2 \gg \omega_1$, the denominator can be approximated by $\omega_2\chi_2$, leading to

$$t_c \approx \frac{\chi(t)}{\omega_2\chi_2}. \tag{14}$$

B. The Baier-Katkov formalism

The approach used in our calculation is the so-called semiclassical operator method developed by Baier and Katkov in the 1960s [31]. This approach is a well-established method that is suitable for calculating QED processes for ultrarelativistic particles in strong background fields, where the motion of the particle can be described classically, while the photon quantum recoil is accounted for. The radiation spectrum reads

$$dI = \frac{\alpha}{(2\pi)^2\tau}\left[-\frac{\varepsilon'^2+\varepsilon^2}{2\varepsilon'^2}|\mathcal{T}_\mu|^2 + \frac{m^2\omega^2}{2\varepsilon'^2\varepsilon^2}|\mathcal{I}|^2\right]d^3\mathbf{k}, \tag{15}$$

where $\mathcal{I} \equiv \int_{-\infty}^{\infty} e^{i\psi}dt$ and $\mathcal{T}_\mu \equiv \int_{-\infty}^{\infty} v_\mu(t)e^{i\psi}dt$, with $\psi \equiv \frac{\varepsilon}{\varepsilon'}k\cdot x(t)$ being the emission phase and $x_\mu(t)$, $v_\mu(t)$, $k_\mu = (\omega, \mathbf{k})$ being the four-vectors of the electron coordinate, the velocity, and the photon momentum, respectively; τ is the pulse duration, ε is the electron energy in the field, and $\varepsilon' = \varepsilon - \omega$.

The actual calculation takes two steps. First, the Lorentz equation for a single particle is solved, and the trajectory is obtained. Second, the time integration in the photon emission amplitude is calculated using the time-dependent momentum and coordinate of the particle. Both steps can proceed either analytically when an analytical trajectory is available or numerically for general laser field and electron beam parameters. Below we will give an analytical derivation of the spectrum using the approximated trajectory of the electron in the CPW scenario.

Let us first look at the phase ψ of the emission, which is a crucial parameter in the formalism and determines the interference of radiation emerging from different points of the trajectory. Introducing the definition of $u = \omega/(\varepsilon - \omega)$, we have

$$\psi = m\gamma u[t - \boldsymbol{n} \cdot \boldsymbol{x}(t)]. \tag{16}$$

The trajectory in the vicinity of t_0 can be represented as

$$\boldsymbol{x}(t_0 + \tau) = \boldsymbol{x}_0 + \boldsymbol{\beta}(t_0)\tau + \int_0^\tau d\tau'[\boldsymbol{\beta}(t_0 + \tau') - \boldsymbol{\beta}(t_0)], \tag{17}$$

with $\boldsymbol{x}_0 = \boldsymbol{x}(t_0)$. Therefore the phase reads

$$\psi = mu\gamma\left[[1 - \beta(t_0)]\tau - \boldsymbol{\beta}(t_0) \cdot \int^\tau d\tau'[\boldsymbol{\beta}(t_0 + \tau') - \boldsymbol{\beta}(t_0)]\right]$$
$$\approx mu\gamma\left[\frac{1}{2\gamma^2}\tau + \int^\tau d\tau' \Lambda(t_0, \tau')\right], \tag{18}$$

where $\boldsymbol{n} \approx \boldsymbol{\beta}(t_0)$ is assumed, i.e., forward emission for the ultrarelativistic electron, and $\Lambda(t_0, \tau) \equiv -\boldsymbol{\beta}(t_0) \cdot [\boldsymbol{\beta}(t_0 + \tau) - \boldsymbol{\beta}(t_0)]$. The constant phase $m\gamma u(t_0 - \boldsymbol{n} \cdot \boldsymbol{x}_0)$ is omitted as it does not affect the interference. In order to understand the physical meaning of $\Lambda(t_0, \tau)$, we rewrite it in the following way:

$$\Lambda(t_0, \tau) = -\beta^2(t_0)[\cos\theta(\tau) - 1] \approx \tfrac{1}{2}\beta^2(t_0)\theta^2(\tau), \tag{19}$$

where $\theta(\tau) \ll 1$ is the angle between $\boldsymbol{\beta}(t_0 + \tau)$ and $\boldsymbol{\beta}(t_0)$. Having expressed the phase ψ in terms of θ and recalling the well-known fact that the radiation formation interval corresponds to $\theta(\tau) \lesssim 1/\gamma$, the formation time may be instantly obtained.

Let us find an explicit expression for the formation time according to the LCFA, corresponding to expanding the velocity up to the τ^2 order, namely,

$$\Lambda(t_0, \tau) = -\frac{1}{2}[\boldsymbol{\beta}(t_0) \cdot \ddot{\boldsymbol{\beta}}(t_0)]\tau^2 = \frac{1}{2}|\dot{\beta}|^2\tau^2 = \frac{m^2\chi^2}{2\gamma^4}\tau^2, \tag{20}$$

where we have assumed that the force acting on the electron is transverse $\boldsymbol{\beta}(t_0) \cdot \dot{\boldsymbol{\beta}}(t_0) = 0$, and the definition of the quantum parameter $\chi = \gamma^2|\dot{\boldsymbol{\beta}}|/m$ was employed. Combining Eqs. (19) and (20), the time dependence of the angle according to the LCFA reads

$$\theta_L(\tau) = \frac{m\chi}{\gamma^2}\tau. \tag{21}$$

Therefore the LCFA formation time, defined by $\theta(t_f^L) = 2/\gamma$, is given by

$$t_f^L = \frac{2\gamma}{m\chi}. \tag{22}$$

This also gives the typical energy of the emitted photon from the condition $\psi \sim 1$. Accordingly, in order to determine for a given trajectory whether a coincidence with LCFA is to be expected or not, one should examine the temporal behavior of the angle $\theta(\tau)$ during the emission interval. A linear dependence indicates a good agreement with LCFA. Moreover, the formation time determines the LCFA applicability via $t_f^L \ll t_c$. Thus the LCFA condition in the CPW setup is

$$\frac{t_f^L}{t_c} \approx \frac{2\gamma\omega_2\chi_2}{m\chi^2(t)} \ll 1, \tag{23}$$

which reduces to the familiar result $t_f^L/t_c \sim 1/\xi$ in a single laser wave.

Now, according to the trajectory given above, the radiation spectral distribution can be represented in the following form:

$$\frac{dI}{d\omega d\varphi} = \frac{\alpha\omega}{4\pi\bar{v}_z(1+u)}\sum_{s_r}\sum_{s_l}\left[-(2+2u+u^2)|\mathcal{M}_\mu|^2 + \left(\frac{u}{\gamma}\right)^2|\mathcal{M}_0|^2\right]. \tag{24}$$

In the following, the matrix element $\mathcal{M}_\mu$ is given as a function of s_l, s_r, u, φ. We start by introducing the quantities

$$\begin{aligned} B_0(s, z, \varphi) &= J_s(z)e^{-is\varphi}, \\ B_1(s, z, \varphi) &= \left[\frac{s}{z}J_s(z)\cos\varphi + iJ_s'(z)\sin\varphi\right]e^{-is\varphi}, \\ B_2(s, z, \varphi) &= \left[\frac{s}{z}J_s(z)\sin\varphi - iJ_s'(z)\cos\varphi\right]e^{-is\varphi}, \end{aligned} \tag{25}$$

where $J_s(z)$ and $J_s'(z)$ are the Bessel function and its first derivative, respectively. In terms of these functions, the various components of the matrix element take the form

$$\begin{aligned} \mathcal{M}_t &= \sum_{s_3} B_0(\mathbf{1})B_0(\mathbf{2})B_0(\mathbf{3}), \\ \mathcal{M}_x &= \frac{m}{\varepsilon}\sum_{s_3}[\xi_1 B_0(\mathbf{2})B_1(\mathbf{1}) + \xi_2 B_0(\mathbf{1})B_1(\mathbf{2})]B_0(\mathbf{3}), \\ \mathcal{M}_y &= \frac{m}{\varepsilon}\sum_{s_3} m[\xi_1 B_0(\mathbf{2})B_2(\mathbf{1}) + \xi_2 B_0(\mathbf{1})B_2(\mathbf{2})]B_0(\mathbf{3}), \\ \mathcal{M}_z &= \sum_{s_3} B_0(\mathbf{1})B_0(\mathbf{2})\left[\bar{v}_z B_0(\mathbf{3}) - \frac{m^2\xi_1\xi_2}{\bar{v}_z\varepsilon^2}B_1(\mathbf{3})\right], \end{aligned} \tag{26}$$

where $\mathbf{1} \equiv (s_1, z_1, \varphi)$, $\mathbf{2} \equiv (s_2, z_2, \varphi)$, and $\mathbf{3} \equiv (s_3, z_3, 0)$. The indices s_1, s_2, s_3 are related to s_r, s_l that appear in the final emission expression by

$$s_1 \equiv s_l - s_3, \quad s_2 \equiv s_r + s_3. \tag{27}$$

The arguments of the Bessel function read

$$z_1 \equiv \frac{m\xi_1 u \sin\vartheta}{\omega_1}, \quad z_2 \equiv \frac{m\xi_2 u \sin\vartheta}{\omega_2}, \quad z_3 \equiv \frac{m^2\xi_1\xi_2 u}{\bar{v}_z\Delta\omega\varepsilon}\cos\vartheta.$$

The angle ϑ is expressed in terms of u, s_l, s_r according to

$$\cos\vartheta = \frac{1}{\bar{v}_z}\left[1 - \frac{1}{\varepsilon u}(s_l\omega_1 + s_r\omega_2)\right]. \tag{28}$$

From Eq. (13) one can see that a small time scale t_c appears in the case of $\chi(t) \to 0$ at some time moment t, which according to Eq. (12) requires $\chi_1 \sim \chi_2$. In the following, the emitted spectrum as well as the deviation from LCFA is examined for several regimes.

III. VIOLATION OF THE LOCAL CONSTANT FIELD APPROXIMATION

Low-ξ_2 case. The radiation spectra for $\xi_1 = 300$ and $\xi_2 = 0.35$ are shown in Fig. 2. We consider three electron energies $\varepsilon = 4.6m_*$, $16.9m_*$, and $40.2m_*$, yielding different dynamics. In the case of $\varepsilon = 4.6m_*$, the ξ_1 beam dominates the dynamics because $\chi_1 > \chi_2$. As $\xi_1 \gg 1$, the angle $\theta(t)$ grows linearly within the $1/\gamma$ cone as in the LCFA; Fig. 2(a). Hence the

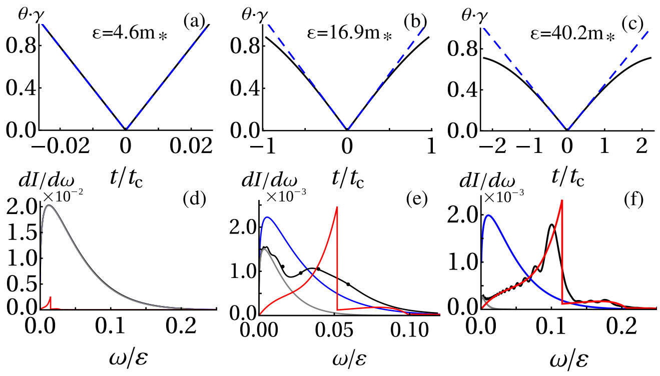

FIG. 2. Results for $\xi_1 = 300$ and $\xi_2 = 0.35$ with energies $\varepsilon = 4.6m_*$ [(a) and (d)], $\varepsilon = 16.9m_*$ [(b) and (e)], and $\varepsilon = 40.2m_*$ [(c) and (f)], respectively. (a)–(c) Solid (dashed) lines for the magnitude of $\theta(t)$ [$\theta_L(t)$ for LCFA] in the vicinity of t_0 when χ is maximal, with always $\theta(t) < \theta_L(t)$ here [$t_c/T = 0.8$, 0.14, and 0.09 for (a)–(c), respectively, with $T = 2\pi/\omega_0$]. (d)–(f) Radiation spectra: Black (blue) is via the analytical trajectory [LCFA with time-dependent $\chi(t)$]; gray and red are for the single beam of ξ_1 and ξ_2, respectively (the electron energy in a single beam is the same as for CPWs). While all the curves are overlapped in (d) except the red one, the gray curve in (f) is rather small compared with the other curves. The spectrum via fully numerical trajectory is shown as black dots in (e).

emitted spectrum in Fig. 2(d) coincides with the LCFA result and is close to the spectrum of the single ξ_1 beam.

For high energy $\varepsilon = 40.2m_*$, the ξ_2 beam is dominant, and therefore $t_f^L/t_c \approx 1/\xi_2 = 2.86$. The angle oscillates inside the $1/\gamma$ cone; Fig. 2(c). The radiation is similar to the case of the electron motion in the ξ_2 beam with a renormalized energy due to the influence of the ξ_1 [Fig. 2(f)]. The typical energy of the emitted photon derived from $\psi \sim 1$ is $\omega = 2\gamma^2\omega_2 \approx 4\gamma^2\omega_0$.

Most interesting is the case of the intermediate energy $\varepsilon = 16.9m_*$. Both beams influence the dynamics as χ_1 and χ_2 are comparable. The ratio t_f^L/t_c oscillates in time and is larger than unity, which indicates the deviation from LCFA. This can be seen from Fig. 2(b), where more than one t_c period contributes to the radiation during the electron oscillation within the $1/\gamma$ cone; see the schematic trajectory in Fig. 1(a). The spectrum [Fig. 2(e)] reveals the qualitative deviations from LCFA, as well as from those in single ξ_1 or ξ_2 beams. This evidences that even in a strong field ($\xi_1 \gg 1$), the LCFA may yield severe errors due to the presence of other weak waves, in contradiction to the LCFA hypothesis.

High-ξ_2 case. The LCFA violation can also be demonstrated with both lasers as strong as $\xi_1 = 300$ and $\xi_2 = 2$. Since nontrivial radiation spectra are found when $\chi_1 \sim \chi_2$ as in Fig. 2(e), we choose $\varepsilon = 6.57m_*$ here so that $\chi_1 \sim \chi_2 \sim 0.025$. From Fig. 3(a) one can see that t_f^L/t_c is far above unity in the vicinity of the smallest $\chi(t)$ regime. This corresponds to the appearance of the smallest typical time scale in the trajectory [$t_3 = \chi_{\min}/(\chi_2\omega_2) \ll 1/\omega_2 = t_2$] as illustrated in Fig. 1(b) and leads to deviation from the LCFA predictions in the entire spectrum [Fig. 3(b)]. Note that the emission in a single wave ξ_1 (gray) or ξ_2 (red) here can be described rather well with the LCFA.

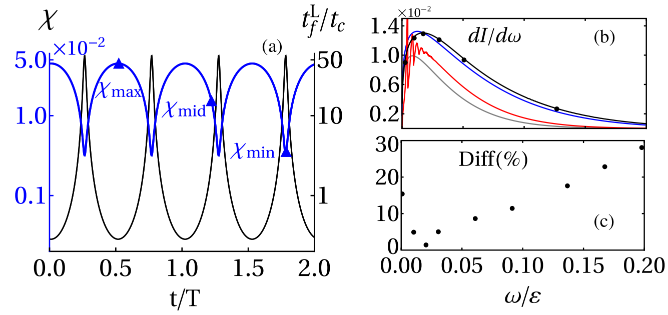

FIG. 3. (a) Instantaneous $\chi(t)$ and t_f^L/t_c vs time t; (b) radiation spectrum. The spectra corresponding to ξ_1 (gray) and ξ_2 (red) are both smaller than the total spectrum (black); (c) the relative difference (Diff) between the BK spectrum and the LCFA one. The electron energy is $\varepsilon = 6.57m_*$. The field intensities are $\xi_1 = 300$ and $\xi_2 = 2$, and the color code is like that in Fig. 2. The triangles $\chi_{\max}$, $\chi_{\rm mid}$, and $\chi_{\min}$ indicate the maximum, middle, and minimum values of the quantum parameter.

We analyze the deviation from the LCFA results in detail for three different directions of emission (see Fig. 4). For clarity, we avoid the interference by only looking at the emission from one cycle of ξ_1. From Figs. 4(a) and 4(d) one notes that in the vicinity of $\chi_{\max}$ the time-dependent angle $\theta(t)$ and the spectrum agree well with the LCFA prediction, because at this point $t_f^L/t_c = 0.28$ [cf. the emission at t_2 in Fig. 1(b)]. Around $\chi_{\rm mid}$, however, the particle oscillates in the $1/\gamma$ cone; see Fig. 4(b). Accordingly, the emitted spectrum does not agree with LCFA results but rather features a harmonic structure [Fig. 4(e)].

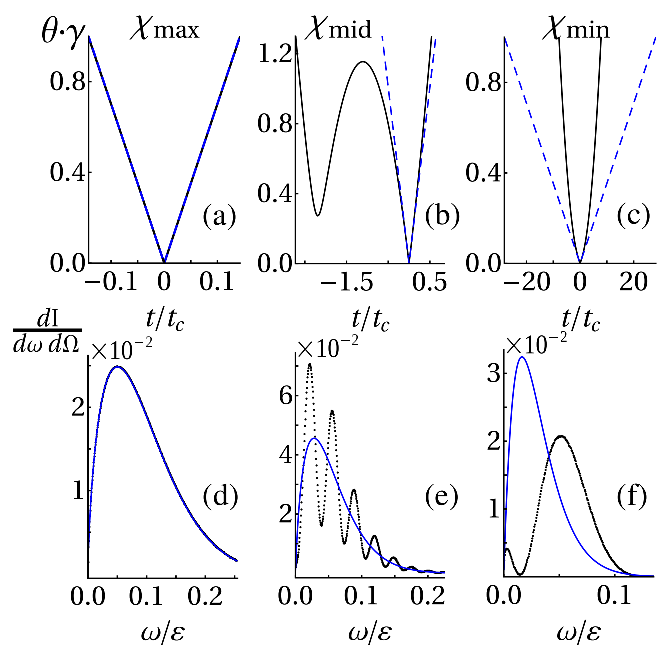

FIG. 4. (a)–(c)The magnitude of $\theta(t)$ for different χ in time as shown in Fig. 3(a), with $t_c = 0.15T$ (a), $t_c = 0.08T$ (b), and $t_c = 0.01T$ (c). (d)–(f) angular-resolved spectra along the emitting directions corresponding to the same χ values. All the other parameters and the color code are like those in Fig. 3.

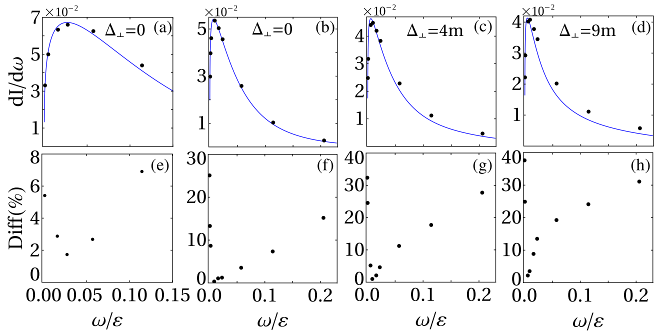

FIG. 5. Results for $\xi_1 = 300$ and $\xi_2 = 10$ with three different transverse momentum spreadings of the electron beam: $\Delta_\perp = 0$ [(a), (b), (e), and (f)], $\Delta_\perp = 4m$ [(c) and (g)], and $\Delta_\perp = 9m$ [(d) and (h)], respectively. (a)–(d) Radiation spectra: black dots (blue lines) are the BK (LCFA) spectra based on the numerical trajectory. (e)–(h) The relative difference between the BK spectrum and the LCFA one. The electron energy is $\varepsilon = 875m$. While a plane wave for the two laser pulses is used in (a) and (e), a realistic pulse shape with $\sin^2$ envelope in time is employed for the others. The pulse duration is 4 cycles for ξ_1 and 20 cycles for ξ_2. The waist size is $5\lambda_0$ for both laser pulses.

An unusual behavior emerges near $\chi_{\min}$. The angle $\theta(t)$ [Fig. 4(c)] increases more rapidly than $\theta_L(t)$. Namely, the deviation stems from the fact that the particle exits the $1/\gamma$-cone much quicker than LCFA predicts [cf. the emission at t_3 in Fig. 1(b)], consequently, the spectrum in Fig. 4(f) is broad and smooth, as opposed to the harmonic structure in Fig. 4(e). This anomalous LCFA violation is qualitatively distinct from the one observed in a monochromatic plane wave and is determined by the condition $t_f \ll t_f^L$; see Fig. 3(a). Due to the smallness of t_f, the typical energy of the emitted photons ω_c in Fig. 4(f) is considerably larger than in LCFA. We estimate it from the condition $\psi \sim 1$:

$$\omega_c \simeq \frac{2m\gamma^2}{mt_f\Theta/2 + 2\gamma} \approx \frac{2m\gamma^2}{mt_f + 2\gamma}, \tag{29}$$

with $\Theta = 1 + (\gamma^2/t_f)\int_{t_f}\theta^2(t')dt' \approx 2$, which provides $\omega_c \approx 0.08\varepsilon$ for the applied parameters, in agreement with Fig. 4(f). Furthermore, the spectra shown in Figs. 4(d)–4(f) have similar amplitudes, explaining the high-energy deviations in Fig. 3(b).

The described deviation from LCFA predictions persists even at higher laser intensities, as shown in the case of $\xi_1 = 300$ and $\xi_2 = 10$ in Fig. 5, albeit the emission of each single beam can be well represented with the LCFA. Here, the realistic electron beam has a transverse momentum spread up to $\Delta_\perp/p \approx 10^{-2}$ with also a realistic Gaussian laser pulse shape except for Figs. 5(a) and 5(e). By comparing Figs. 5(a) and 5(e) with Figs. 5(b) and 5(f), we can see that the deviation with respect to LCFA results is even enhanced in a realistic setup. In particular, the deviation is larger with increased spreading of the electron momentum, and the relative difference in the high-energy domain can be around 30% [Figs. 5(f)–5(h)].

The increase in the relative difference in the high-energy domain has a simple explanation. In this anomalous LCFA violation, $t_f^L > t_f$, which means that the typical emitted frequencies are smaller in the LCFA case $\omega_c^L < \omega_c$, or the peak of the LCFA spectrum is at lower frequencies. From another side, in the high-frequency domain the spectrum is exponentially damped $\frac{dI}{d\omega d\Omega} \propto \exp[-t_f/t_{\rm coh}(\omega)]$, with the coherence time $t_{\rm coh}(\omega) \equiv \pi/(\omega - \boldsymbol{k}\cdot\boldsymbol{v})$ [57]. This means that for small ω, LCFA overestimates the emission, while for large ω, LCFA underestimates it, and the relative difference will first decrease with the increase in the radiation energy and then increase after the frequency of the emitted photon exceeds ω_c.

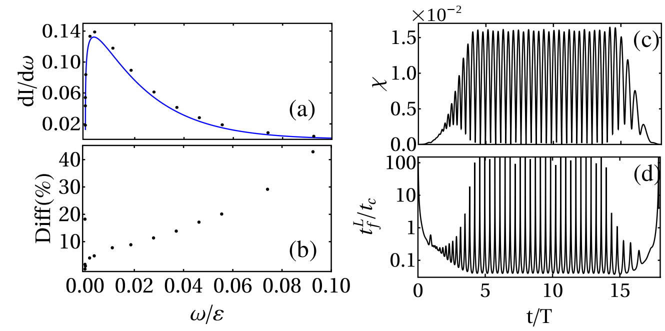

FIG. 6. The radiation of an electron trapped in a CPW with $\xi_1 = 100$ and $\xi_2 = 50$: (a) radiation spectrum (blue line is the result via the LCFA, while dots represent the results according to the numerical trajectory); (b) relative difference between the precise numerical spectrum and that via the LCFA; (c) quantum parameter $\chi(t)$ as a function of time; and (d) t_f^L/t_c as a function of time. The average energy ε equals $54m$.

The intensity of the laser pulses and the energy of the electrons in the calculations are chosen such that the quantum parameter regarding each laser pulse χ_1 and χ_2 are of the same order of magnitude and that the maximal value of $\chi(t)$ is of the order of $\sim$0.01–0.1. The emitted photon energy can reach $\sim$10–20% of the electron energy, indicating the quantum regime of interaction, and the radiation reaction is not very significant, when the energy emitted during a laser cycle (estimated via $R = \alpha\xi\chi \lesssim 0.2$ [3]) is small but not negligible. However, the role of radiation reaction is not essential for the deviation of the BK spectra with respect to those with the LCFA, because the LCFA results are also disturbed by radiation reaction.

Trapping case. Next, we consider two laser fields with comparable amplitudes $\xi_1 = 100$ and $\xi_2 = 50$. In this setup, the electron can be trapped in a certain region provided the initial energy is smaller than the potential well created by the two lasers. Accordingly, $\bar{\beta}_z = 0$, so the analytical solution employed above is not valid, and we rely on numerical calculations. However, the qualitative picture remains the same, i.e., χ is oscillating as shown in Fig. 6(c), and near its minima the LCFA condition is violated; see Fig. 6(d). As a result, this anomalous LCFA violation appears in the spectrum [Figs. 6(a) and 6(b)], similar to those demonstrated for the intermediate- and high-ξ_2 calculations. However, as opposed to these cases, the LCFA deviation shows only weak sensitivity to the electron momentum, as long as it is not energetic enough to escape the trapping. Therefore the violation in this scenario is rather robust.

Ultrashort pulse. An analogous deviation from LCFA predictions due to the emergence of a small characteristic time scale in the electron trajectory can also happen in a simpler

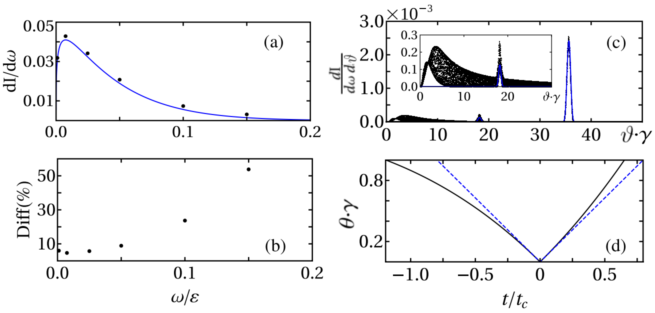

FIG. 7. Radiation in an ultrashort laser pulse: (a) The spectrum with LCFA (blue) and BK method (black). (b) The relative difference between the BK result and the LCFA one. (c) Angular-resolved spectrum with a fixed azimuthal direction $\varphi = 3\pi/4$ and for $\omega = 10m$; the inset is a zoom-in between $\vartheta = 0$ and $30/\gamma$. (d) The magnitude of $\theta(t)$ for $t_0 = -0.65T$ corresponding to $\gamma\vartheta = 1.25$ in (c). The ultrashort laser pulse has a Gaussian profile with a standard deviation $\sigma = \pi$ and $\xi = 50$ at $t = 0$. The waist size is $w_0 = 3\lambda_0$. The electron with energy of $100m$ counterpropagates with the laser pulse.

field configuration. We have analyzed the radiation emitted by an ultrarelativistic electron colliding with a single ultrashort laser pulse, where the characteristic time scale of the electron trajectory is shaped not only by the central frequency of the laser wave but also by the time envelope of the laser pulse. A comparison of the BK radiation spectra calculated numerically with those via the LCFA is presented in Fig. 7.

Surprisingly, even though $\xi = 50 \gg 1$, a difference between the LCFA prediction and the BK result exists through the entire spectrum, including for high energies [see Figs. 7(a) and 7(b)]. To seek the reason for the deviation, the angular-resolved spectrum with a fixed azimuthal direction $\varphi = 3\pi/4$ for the emitted energy $\omega = 0.1\varepsilon = 10m$ is displayed in Fig. 7(c). One can see that the main difference corresponds to a low ϑ value [see the inset of Fig. 7(c)], namely, at the beginning and the end of the trajectory, where the direction of motion is changing rapidly [see Fig. 7(d)], in accordance with this anomalous violation. The corresponding characteristic time $t_c = 0.0613T$ for $\gamma\vartheta = 1.25$ in Fig. 7(c) is rather small compared with the laser period, and thus $t_f^L/t_c = 1.59 > 1$, as $\dot{\boldsymbol{F}}$ is large and $\boldsymbol{F}$ is small at the beginning and the end of the ultrashort pulse ($t_c = |\boldsymbol{F}|/|\dot{\boldsymbol{F}}|$). Therefore, similar to the CPW case of Fig. 4(f), the rise and the fall of the ultrashort laser pulse can influence the emission in the whole spectral range, even though the quantum parameter $\chi(t)$ is relatively small but the ratio $t_f^L/t_c \gg 1$ in this region is large.

IV. CONCLUSION

The state-of-the-art numerical modeling widely used to account for realistic laser-plasma scenarios [particle-in-cell (PIC)-QED codes] commonly relies on the LCFA, which assumes that in strong fields with field parameter $\xi \gg 1$, the radiation and other QED process probabilities coincide with those in a constant crossed field. The justification of its validity is simply deduced from an idealized plane-wave case. As a result, one usually considers the strongest field taking part in the interaction in the kinematic calculation. For example, in the interaction of a high-intensity laser pulse with plasma, numerous electromagnetic modes are expected to arise (various plasma waves as well as reflected waves). Nevertheless, the applicability of the LCFA (as understood in the PIC-QED community) is not affected by these waves but is determined according to the strong driving laser only. The main aim of this paper is to challenge this hypothesis in a multibeam setup, and we have shown explicitly in our simulations (see Fig. 2) that in this situation, even with a strong incident laser with $\xi \gg 1$, the LCFA predictions can be far from the exact results based on the BK method both qualitatively and quantitatively.

Moreover, our findings imply that the widely accepted paradigm regarding the spectrum corresponding to LCFA violation should be revised. All deviations from LCFA explored in the literature, to the best of our knowledge, originate from oscillations of the particle within the formation length [28,32,52–54]. This will induce an additional low-harmonic structure in the infrared tail of the spectrum. However, we have demonstrated a type of LCFA violation featuring broad and smooth corrections to the spectrum with an enhancement in the high-energy domain compared with the LCFA one. This is due to the fact that the electron turns sharply and leaves the formation zone much earlier than in the LCFA estimation, resulting in the appearance of an extremely small t_c in the electron dynamics.

Furthermore, we provide an intuitive condition where this anomalous violation may be encountered. Namely, in the region where $\chi(t)$ becomes small and changes rapidly, this will cause a decrease in t_c and t_f. We explicitly showed above that even though the local χ is low, the contribution to the emission is important (see the angle-resolved spectra in Fig. 4). This condition may occur in various scenarios, as demonstrated in this paper: short pulses, multibeam configurations, and laser-plasma wave interactions (where the particle is accelerated in the direction of the laser pulse and collides with the plasma wave). The combination of the validity criterion in Eq. (23) with the intuitive picture will allow the PIC community to quantitatively estimate the possible impact on full-size simulations.

ACKNOWLEDGMENTS

Q.Z.L and E.R. contributed equally to the work, to numerical and analytical calculations, respectively. E.R. acknowledges partial support from the Alexander von Humboldt Foundation.

[1] G. A. Mourou, T. Tajima, and S. V. Bulanov, Optics in the relativistic regime, Rev. Mod. Phys. **78**, 309 (2006).

[2] M. Marklund and P. K. Shukla, Nonlinear collective effects in photon-photon and photon-plasma interactions, Rev. Mod. Phys. **78**, 591 (2006).

[3] A. Di Piazza, C. Müller, K. Z. Hatsagortsyan, and C. H. Keitel, Extremely high-intensity laser interactions with fundamental quantum systems, Rev. Mod. Phys. **84**, 1177 (2012).

[4] T. Heinzl, Strong-field QED and high-power lasers, Int. J. Mod. Phys. A **27**, 1260010 (2012).

[5] G. V. Dunne, Extreme quantum field theory and particle physics with IZEST, Eur. Phys. J.: Spec. Top. **223**, 1055 (2014).

[6] I. C. E. Turcu, B. Shen, D. Neely, G. Sarri, K. A. Tanaka, P. McKenna, S. P. D. Mangles, T.-P. Yu, W. Luo, X.-L. Zhu, and Y. Yin, Quantum electrodynamics experiments with colliding petawatt laser pulses, High Power Laser Sci. Eng. **7**, e10 (2019).

[7] C. Bula, K. T. McDonald, E. J. Prebys, C. Bamber, S. Boege, T. Kotseroglou, A. C. Melissinos, D. D. Meyerhofer, W. Ragg, D. L. Burke, R. C. Field, G. Horton-Smith, A. C. Odian, J. E. Spencer, D. Walz, S. C. Berridge, W. M. Bugg, K. Shmakov, and A. W. Weidemann, Observation of Nonlinear Effects in Compton Scattering, Phys. Rev. Lett. **76**, 3116 (1996).

[8] D. L. Burke, R. C. Field, G. Horton-Smith, J. E. Spencer, D. Walz, S. C. Berridge, W. M. Bugg, K. Shmakov, A. W. Weidemann, C. Bula, K. T. McDonald, E. J. Prebys, C. Bamber, S. J. Boege, T. Koffas, T. Kotseroglou, A. C. Melissinos, D. D. Meyerhofer, D. A. Reis, and W. Ragg, Positron Production in Multiphoton Light-by-Light Scattering, Phys. Rev. Lett. **79**, 1626 (1997).

[9] Y. J. Gu, O. Klimo, S. V. Bulanov, and S. Weber, Brilliant gamma-ray beam and electron–positron pair production by enhanced attosecond pulses, Commun. Phys. **1**, 93 (2018).

[10] B. King, B. M. Dillon, K. A. Beyer, and G. Gregori, Axion-like-particle decay in strong electromagnetic backgrounds, J. High Energy Phys. 12 (2019) 162.

[11] J. M. Cole, K. T. Behm, E. Gerstmayr, T. G. Blackburn, J. C. Wood, C. D. Baird, M. J. Duff, C. Harvey, A. Ilderton, A. S. Joglekar, K. Krushelnick, S. Kuschel, M. Marklund, P. McKenna, C. D. Murphy, K. Poder, C. P. Ridgers, G. M. Samarin, G. Sarri, D. R. Symes *et al.*, Experimental Evidence of Radiation Reaction in the Collision of a High-Intensity Laser Pulse with a Laser-Wakefield Accelerated Electron Beam, Phys. Rev. X **8**, 011020 (2018).

[12] K. Poder, M. Tamburini, G. Sarri, A. Di Piazza, S. Kuschel, C. D. Baird, K. Behm, S. Bohlen, J. M. Cole, D. J. Corvan, M. Duff, E. Gerstmayr, C. H. Keitel, K. Krushelnick, S. P. D. Mangles, P. McKenna, C. D. Murphy, Z. Najmudin, C. P. Ridgers, G. M. Samarin *et al.*, Experimental Signatures of the Quantum Nature of Radiation Reaction in the Field of an Ultraintense Laser, Phys. Rev. X **8**, 031004 (2018).

[13] X. S. Geng, L. L. Ji, B. F. Shen, B. Feng, Z. Guo, Q. Yu, L. G. Zhang, and Z. Z. Xu, Quantum reflection above the classical radiation-reaction barrier in the quantum electro-dynamics regime, Commun. Phys. **2**, 66 (2019).

[14] D. Strickland, Nobel Lecture: Generating high-intensity ultrashort optical pulses, Rev. Mod. Phys. **91**, 030502 (2019).

[15] G. Mourou, Nobel Lecture: Extreme light physics and application, Rev. Mod. Phys. **91**, 030501 (2019).

[16] J. W. Yoon, C. Jeon, J. Shin, S. K. Lee, H. W. Lee, I. W. Choi, H. T. Kim, J. H. Sung,, and C. H. Nam, Achieving the laser intensity of 5.5×10^{22} W/cm^2 with a wavefront-corrected multi-PW laser, Opt. Express **27**, 20412 (2019).

[17] The Vulcan facility, https://www.clf.stfc.ac.uk/Pages/Vulcan.aspx.

[18] The Extreme Light Infrastructure (ELI), https://www.eli-laser.eu/.

[19] Exawatt Center for Extreme Light Stidies (XCELS), http://www.xcels.iapras.ru/.

[20] D. M. Wolkow, Über eine Klasse von Lösungen der Diracschen Gleichung, Z. Phys. **94**, 250 (1935).

[21] A. Di Piazza, Ultrarelativistic Electron States in a General Background Electromagnetic Field, Phys. Rev. Lett. **113**, 040402 (2014).

[22] R. Blankenbecler and S. D. Drell, Quantum treatment of beamstrahlung, Phys. Rev. D **36**, 277 (1987).

[23] V. G. Bagrov and D. Gitman, *Exact Solutions of Relativistic Wave Equations*, Mathematics and Its Applications Vol. 39 (Springer, New York, 1990).

[24] N. V. Elkina, A. M. Fedotov, I. Yu. Kostyukov, M. V. Legkov, N. B. Narozhny, E. N. Nerush, and H. Ruhl, QED cascades induced by circularly polarized laser fields, Phys. Rev. Spec. Top.–Accel. Beams **14**, 054401 (2011).

[25] C. P. Ridgers, J. G. Kirk, R. Duclous, T. G. Blackburn, C. S. Brady, K. Bennett, T. D. Arber, and A. R. Bell, Modelling gamma-ray photon emission and pair production in high-intensity laser-matter interactions, J. Comput. Phys. **260**, 273 (2014).

[26] D. G. Green and C. N. Harvey, SIMLA: Simulating particle dynamics in intense laser and other electromagnetic fields via classical and quantum electrodynamics, Comput. Phys. Commun. **192**, 313 (2015).

[27] A. Gonoskov, S. Bastrakov, E. Efimenko, A. Ilderton, M. Marklund, I. Meyerov, A. Muraviev, A. Sergeev, I. Surmin, and E. Wallin, Extended particle-in-cell schemes for physics in ultrastrong laser fields: Review and developments, Phys. Rev. E **92**, 023305 (2015).

[28] A. Di Piazza, M. Tamburini, S. Meuren, and C. H. Keitel, Implementing nonlinear Compton scattering beyond the local-constant-field approximation, Phys. Rev. A **98**, 012134 (2018).

[29] T. G. Blackburn, D. Seipt, S. S. Bulanov, and M. Marklund, Radiation beaming in the quantum regime, Phys. Rev. A **101**, 012505 (2020).

[30] e and m are the electron charge and mass, respectively.E_0, $F^{\mu\nu}$, and ω_0 are the laser field amplitude, field tensor, and frequency, respectively ($\omega_0 = 1.55$ eV and units $\hbar = c = 1$ are used throughout). $\varepsilon = m\gamma$ and P_ν are the electron energy and four-momentum, respectively.

[31] V. N. Baier, V. M. Katkov, and V. M. Strakhovenko, *Electromagnetic Processes at High Energies in Oriented Single Crystals* (World Scientific, Singapore, 1994).

[32] V. I. Ritus, Quantum effects of the interaction of elementary particles with an intense electromagnetic field, J. Sov. Laser Res. **6**, 497 (1985).

[33] J. D. Jackson, *Classical Electrodynamics* (Wiley, New York, 1975).

[34] In a circularly polarized monochromatic plane wave, the trajectory of an electron in the average rest frame is a circle with $\gamma = \xi$ [58]. When $\xi \gg 1$, the formation length is $\ell_f \sim \rho\theta \sim \rho/\gamma$, with the radius of the trajectory ρ, and the angle of the coherent emission $\theta \sim 1/\gamma$. The typical length scale of the trajectory in this case is $\ell_c = \rho$. Therefore $t_f/t_c = \ell_f/\ell_c \sim 1/\xi \ll 1$ is automatically fulfilled at $\xi \gg 1$ in a single laser field.

[35] C. S. Brady, C. P. Ridgers, T. D. Arber, A. R. Bell, and J. G. Kirk, Laser Absorption in Relativistically Underdense Plasmas by Synchrotron Radiation, Phys. Rev. Lett. **109**, 245006 (2012).

[36] S. S. Bulanov, V. D. Mur, N. B. Narozhny, J. Nees, and V. S. Popov, Multiple Colliding Electromagnetic Pulses: A Way to Lower the Threshold of e^+e^- Pair Production from Vacuum, Phys. Rev. Lett. **104**, 220404 (2010).

[37] I. Gonoskov, A. Aiello, S. Heugel, and G. Leuchs, Dipole pulse theory: Maximizing the field amplitude from 4π focused laser pulses, Phys. Rev. A **86**, 053836 (2012).

[38] A. Gonoskov, A. Bashinov, S. Bastrakov, E. Efimenko, A. Ilderton, A. Kim, M. Marklund, I. Meyerov, A. Muraviev, and A. Sergeev, Ultrabright GeV Photon Source via Controlled Electromagnetic Cascades in Laser-Dipole Waves, Phys. Rev. X **7**, 041003 (2017).

[39] J. Magnusson, A. Gonoskov, M. Marklund, T. Zh. Esirkepov, J. K. Koga, K. Kondo, M. Kando, S. V. Bulanov, G. Korn, C. G. R. Geddes, C. B. Schroeder, E. Esarey, and S. S. Bulanov, Multiple colliding laser pulses as a basis for studying high-field high-energy physics, Phys. Rev. A **100**, 063404 (2019).

[40] J. G. Kirk, A. R. Bell, and I. Arka, Pair production in counter-propagating laser beams, Plasma Phys. Controlled Fusion **51**, 085008 (2009).

[41] T. Grismayer, M. Vranic, J. L. Martins, R. A. Fonseca, and L. O. Silva, Laser absorption via quantum electrodynamics cascades in counter propagating laser pulses, Phys. Plasmas **23**, 056706 (2016).

[42] M. Jirka, O. Klimo, S. V. Bulanov, T. Zh. Esirkepov, E. Gelfer, S. S. Bulanov, S. Weber, and G. Korn, Electron dynamics and γ and e^-e^+ production by colliding laser pulses, Phys. Rev. E **93**, 023207 (2016).

[43] Z. Gong, R. H. Hu, Y. R. Shou, B. Qiao, C. E. Chen, X. T. He, S. S. Bulanov, T. Zh. Esirkepov, S. V. Bulanov, and X. Q. Yan, High-efficiency γ-ray flash generation via multiple-laser scattering in ponderomotive potential well, Phys. Rev. E **95**, 013210 (2017).

[44] T. Grismayer, M. Vranic, J. L. Martins, R. A. Fonseca, and L. O. Silva, Seeded QED cascades in counterpropagating laser pulses, Phys. Rev. E **95**, 023210 (2017).

[45] M. M. Dellweg and C. Müller, Spin-Polarizing Interferometric Beam Splitter for Free Electrons, Phys. Rev. Lett. **118**, 070403 (2017).

[46] S. Gales, K. A. Tanaka, D. L. Balabanski, F. Negoita, D. Stutman, O. Tesileanu, C. A. Ur, D. Ursescu, I. Andrei, S. Ataman, M. O. Cernaianu, L. D'Alessi, I. Dancus, B. Diaconescu, N. Djourelov, D. Filipescu, P. Ghenuche, D. G. Ghita, C. Matei, K. Seto *et al.*, The extreme light infrastructure—nuclear physics (ELI-NP) facility: New horizons in physics with 10 PW ultra-intense lasers and 20 MeV brilliant gamma beams, Rep. Prog. Phys. **81**, 094301 (2018).

[47] B. Rus, P. Bakule, D. Kramer, J. Naylon, J. Thoma, M. Fibrich, J. T. Green, J. C. Lagron, R. Antipenkov, J. Bartoníček, F. Batysta, R. Baše, R. Boge, S. Buck, J. Cupal, M. A. Drouin, M. Ďurák, B. Himmel, T. Havlíček, P. Homer *et al.*, ELI-beamlines: progress in development of next generation short-pulse laser systems, in *Research Using Extreme Light: Entering New Frontiers with Petawatt-Class Lasers III*, Proceedings of SPIE Vol. 10241 (International Society for Optics and Photonics, Bellingham, WA, 2017), p. 102410J.

[48] B. Shen, Z. Bu, J. Xu, T. Xu, L. Ji, R. Li, and Z. Xu, Exploring vacuum birefringence based on a 100 PW laser and an x-ray free electron laser beam, Plasma Phys. Controlled Fusion **60**, 044002 (2018).

[49] A. Gonoskov, A. Bashinov, I. Gonoskov, C. Harvey, A. Ilderton, A. Kim, M. Marklund, G. Mourou, and A. Sergeev, Anomalous Radiative Trapping in Laser Fields of Extreme Intensity, Phys. Rev. Lett. **113**, 014801 (2014).

[50] J. G. Kirk, Radiative trapping in intense laser beams, Plasma Phys. Controlled Fusion **58**, 085005 (2016).

[51] V. N. Baier, V. M. Katkov, and V. M. Strakhovenko, Quantum radiation theory in inhomogeneous external fields, Nucl. Phys. B **328**, 387 (1989).

[52] M. Kh. Khokonov and H. Nitta, Standard Radiation Spectrum of Relativistic Electrons: Beyond the Synchrotron Approximation, Phys. Rev. Lett. **89**, 094801 (2002).

[53] A. Di Piazza, M. Tamburini, S. Meuren, and C. H. Keitel, Improved local-constant-field approximation for strong-field QED codes, Phys. Rev. A **99**, 022125 (2019).

[54] A. Ilderton, B. King, and D. Seipt, Extended locally constant field approximation for nonlinear Compton scattering, Phys. Rev. A **99**, 042121 (2019).

[55] V. N. Baier and V. M. Katkov, Processes involved in the motion of high energy particles in a magnetic field, Zh. Eksp. Teor. Fiz. **53**, 1478 (1968) [Sov. Phys. JETP **26**, 854 (1968)].

[56] S. Meuren, C. H. Keitel, and A. Di Piazza, Semiclassical picture for electron-positron photoproduction in strong laser fields, Phys. Rev. D **93**, 085028 (2016).

[57] I. I. Abbasov, B. M. Bolotovskii, and V. A. Davydov, High-frequency asymptotic behavior of radiation spectra of moving charges in classical electrodynamics, Usp. Fiz. Nauk **149**, 709 (1986) [Sov. Phys.-Usp. **29**, 788 (1986)].

[58] E. S. Sarachik and G. T. Schappert, Classical theory of the scattering of intense laser radiation by free electrons, Phys. Rev. D **1**, 2738 (1970).